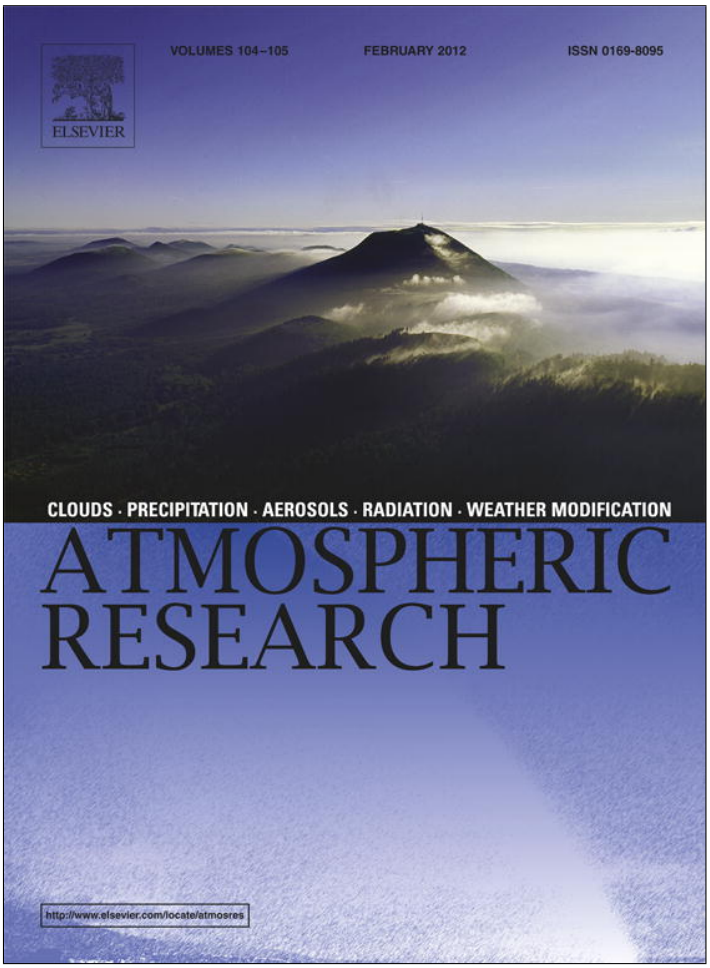

Atmospheric Research 104–105 (2012) 119–127

Contents lists available at SciVerse ScienceDirect

Atmospheric Research

journal homepage: www.elsevier.com/locate/atmos

Comparison of two methodologies for long term rainfall monitoring using a commercial microwave communication system

Asaf Rayitsfeld [a], Rana Samuels [a,*], Artem Zinevich [b], Uri Hadar [c], Pinhas Alpert [a,b]

[a] Geophysics and Planetary Science Department, Tel Aviv University, Ramat Aviv, Israel
[b] The Porter School of Environmental Studies, Tel Aviv University, Ramat Aviv, Israel
[c] School of Electrical Engineering, Tel Aviv University, Ramat Aviv, Israel

ARTICLE INFO

Article history:
Received 1 December 2010
Received in revised form 15 August 2011
Accepted 24 August 2011

Keywords:
Precipitation
Precipitation measurements
Microwave links

ABSTRACT

Rainfall measurements have been investigated worldwide because of their important implications in meteorology, hydrology, flood warnings and fresh water resource management. Recently a new way of measuring rainfall based on commercial microwave radio links that form cellular communication networks has been proposed, in which the path-integrated rainfall intensity is estimated from the received signal level. This method can reveal fine-scale evolution of rainfall in space and time and allows observation of near-surface rainfall at a spatial resolution of up to 1×1 km^2 and a temporal resolution of up to 1 min, with no additional installation and maintenance costs. Here we examine two different methodologies for calculating instantaneous rainfall from microwave links. The study region covers a 1600 km^2 area in central Israel which includes up to 70 commercial microwave links, and 7 rain gauges installed in the vicinity of the links. 19 rainstorm events over a two year period covering about a 676 h overall period, are evaluated. The first methodology uses data from the nearest microwave link while the second uses data interpolated at the point of the rain gauge from multiple nearby links. Results are compared to results from nearby rain gauges. At temporal resolutions of 1 min correlations of 0.65 and .77, with biases of -0.08 and -0.06 mm h^{-1} were attained for the first and second methods, respectively. At the temporal resolution of 10 min, the correlations of 0.84 and 0.85, with biases of -0.11 and -0.06 mm h^{-1} were attained. On average, application of the interpolation point methodology underestimated accumulated rainfall by only 3% as compared to nearby rain gauges. The single link method overestimated rainfall by 6%. Both methodologies improved (worsened) as the density of the microwave link grid increased (decreased).

1. Introduction

Traditionally, disturbances in microwave radio propagation caused by scattering and absorption of precipitation have been studied in order to optimize reliable Wireless Communication System (WCS) design and planning. Recently, it has been proposed that these same impairments can be used as a novel way to measure rainfall as well as other meteorological phenomena (David et al., 2009; Leijnse et al., 2007a; Messer, 2007; Messer et al., 2006). Given that the attenuation of a radio signal at the frequencies of tens of GHz near wavelengths of 1 cm is dominated by the effects of rainfall, this could serve as a basis for measurements of path-integrated and area-integrated rainfall (Atlas and Ulbrich, 1974; Atlas and Ulbrich, 1977; Jameson, 1991). The power-law equation relates the signal attenuation A [dB km^{-1}] with path-average rainfall intensity R [mm h^{-1}] as

$$A = aR^b \tag{1}$$

where the parameters a and b are, in general, functions of the link's frequency, polarization and Drop Size Distribution (DSD) (Jameson, 1991).

* Corresponding author at: Geophysics and Planetary Science Department, Tel Aviv University, Ramat Aviv, Tel Aviv, 69978, Israel.
E-mail address: ranas@post.tau.ac.il (R. Samuels).

0169-8095/$ – see front matter © 2011 Elsevier B.V. All rights reserved.
doi:10.1016/j.atmosres.2011.08.011

The advantage of microwave links for high temporal resolution measurements over conventional rain gauges has been demonstrated by Minda and Nakamura (2005). Previous works have shown that the use of dual-frequency links, operating on different, specially selected frequencies, allows producing reliable estimates of path-integrated rainfall and rainfall spatial distribution, in conjunction with rain-gauges and radar (Goldshtein et al., 2009; Grum et al., 2005; Holt et al., 2000; Rahimi et al., 2006; Rahimi et al., 2003). Following these findings, a number of applications of microwave measurements have been explored. The potential of use of single-frequency links for urban rainfall measurements was suggested by Upton et al. (2005) and Krämer et al. (2003). Dual-frequency links find applications in calibration of weather radar (Rahimi et al., 2006), correction of X-band radar rainfall estimates (Krämer et al., 2005), identification of melting snow (Upton et al., 2007) and even estimation of DSD parameters (Rincon and Lang, 2002).

The use of microwave attenuation measurements for the tomographic reconstruction of rainfall fields was first suggested by Giuli et al. (1999) who proposed a specially designed hypothesized system of microwave links with predefined geometry, operating at either specially selected frequencies where the A–R relationship is linear, or using differential phase shift. This system allowed application of linear tomography to reconstruct spatial distribution of rainfall. However, all these approaches relied on dedicated, specially installed equipment.

Recent advances in communication technology enable the use of off-the-shelf commercial microwave communication hardware, resulting in no or low costs for the application of this methodology. However, the use of standard, already existing commercial hardware installations poses new challenges, because commercial microwave networks are optimized for high communication performance and are designed in the way that reduces the effect of weather-related impairments on quality of service. Thus, the observation type, time and magnitude resolution, network geometry and frequencies are predefined and, in most cases, cannot be changed; records of Received Signal Level (RSL) are distorted by quantization. Tomographic reconstruction of spatial rainfall intensity distribution from RSL records in commercial microwave networks is addressed by Goldshtein et al. (2009) and Zinevich et al. (2008). Other difficulties are in estimation of average rainfall per link from signal attenuation include uncertainties due to variability of DSD along the link (Berne and Uijlenhoet, 2007), wet antenna attenuation (Leijnse et al., 2007b; Minda and Nakamura, 2005) and uncertainty in determination of clear air attenuation due to water vapor-induced attenuation and scintillation effects (David et al., 2009; Holt et al., 2003; Rahimi et al., 2003).

These previous studies were methodological and/or technically oriented. In this paper, we present an extensive performance evaluation over a statistically representative real-world dataset and compare the results of two different very basic methodologies. This provides both an examination of the techniques proposed as well as a well defined data set for additional research focusing on their improvement. We also present a novel method for determining wet and dry periods from attenuation data using a hidden Markov Model. Here we assess the performance limits of previously proposed techniques by examining 676 h of microwave attenuation data, collected in central Israel over the period of two years (2006–2008) by a standard microwave communication network, comprising up to 70 microwave links, at the temporal resolution of 1 min. The 19 rain events recorded over this period represent the typical Israeli winter rainfall patterns (Shay-Al and Alpert, 1991) and provide a first analysis of the skill of data from microwave links to be used as a proxy for rainfall measurements based on long term data.

2. Study area

The study area is a region in the south-western part of Israel centered around the cities of Ramle, Lod and Modiin covering an area of about 42×44 km^2 (Fig. 1). A total of 70 commercial microwave links and 7 rain gauges were used over a period of 2 years, recording 19 individual rain events (676 h) between mid-December 2006 until February 2008. It should be noted that only a representative subset of the links is shown in the figure to enable readability. Most of the rain events in Israel are intense convective cold fronts, occurring in autumn and winter from October to May (Goldreich, 2003); these constitute the majority of the studied events. The links are part of the operational microwave network of the Israeli cellular provider Pelephone Ltd. The microwave links used are all vertically polarized and operate at the frequency bands 16–24 GHz, with lengths varying from 0.8 to 18 km. The built-in measurement and logging facilities register RSL at the magnitude resolution of 1 dB every minute. Higher resolution of 0.1 dB RSL commercial data was also analyzed in other regions but not with such an extensive spatial and temporal resolution (David et al., 2009; Zinevich et al., 2010).

The density of the links varies considerably even over this small area, reaching its peak around the MTG (Switch, in Hebrew) Ramle in the middle of Ramle city. East of Ramle, however, the density is rather low, a natural consequence of the fact that the density of cellular masts often follows that of the population and is low in suburban areas. The density of the links in the southern part of the map is higher because of the increase in the urban population (around the city of Kiryat Malachi). The installation and operation of the microwave links are dynamic due to technical and economic efficiency considerations.

Over the course of this research, seven tipped-bucket rain gauges TE525MM, measuring with temporal resolution of 1 min (identical to the link's time resolution) and magnitude resolution of 0.1 mm per bucket were placed in the region to provide a measure of comparison and validation of rainfall estimates from the microwave links. Note that due to the removal of the nearby microwave link, the Maccabim rain gauge (RG5) had to be removed at the end of September 2007 and was transferred to Talmie-Yechiel (RG7) near Malachi switch in January 2008. Each rain gauge recorded between 5 and 19 rain events, depending on whether the microwave links were operating at the same time (Table 1).

3. Methodology

In this study, we compare the calculated rainfall from microwave links to measured rainfall from rain gauges. Two basic methodologies for calculating rainfall measurements from microwave links were applied. More sophisticated dynamical interpolation was also tested for some events with

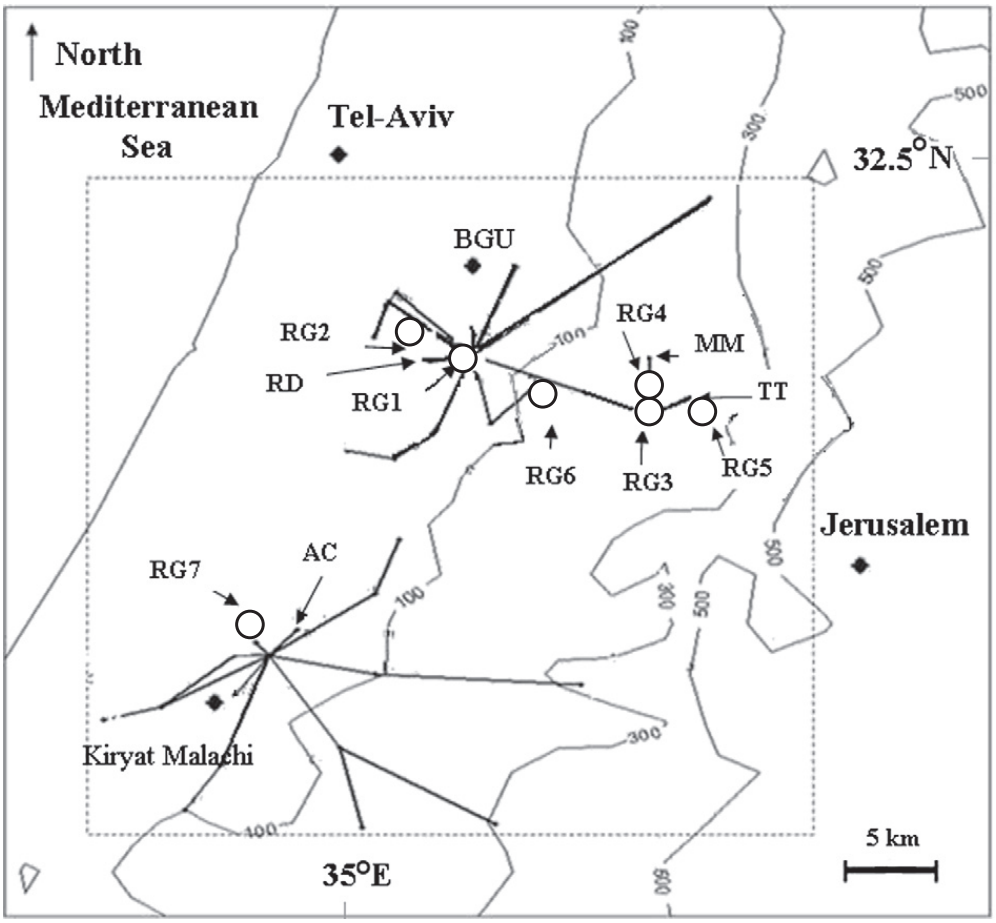

Acronym	Rain gauge name
RG1	MTG Ramle
RG2	Ramle West
RG3	Modiin Center
RG4	Modiin Shimshoni
RG5	Maccabim
RG6	Kfar Shmuel
RG7	Talmei Yechiel

Acronym	Microwave link name
AC	Achva
BGU	Ben Gurion Air port
MM	Mavo Modiin
RD	Ramat Dan
TT	Titora

Fig. 1. Locations of the microwave links, used for rainfall observations, and the locations of the rain gauges (O). The geographic locations of all 7 rain gauges RG1,… RG7 and of other locations are given in the Tables to the right.

some advantages (Zinevich et al., 2009). Both methodologies are based on the use of the power law (Eq. (1)) and are applied after estimating zero level attenuation, described below in Section 3.1. The first methodology, following Messer et al. (2006) and Leijnse et al. (2007a) simply uses RSL data from a single link, applies the power law, and compares results to data from the closest rain gauge. The second methodology, following Goldshtein et al. (2009) uses a modified Inverse Distance Weighted (IDW) interpolation to calculate rainfall at the rain gauge point based on RSL values from all nearby links. This methodology is described briefly below in Section 3.2. More details can be found in Goldshtein et al. (2009).

3.1. Zero level attenuation

While the calculation of rainfall from microwave links is governed by the power law (Eq. (1)), dynamic quantization renders the baseline or 'zero-level' attenuation quite challenging as the attenuation level at the beginning of a rain event might differ from that at the end, introducing a high level of error into the power law calculations. By identifying wet and dry periods before, during and after a rain event from a series of RSL measurements, we can address this challenge by only including 'rain induced attenuation' in the power law calculations. For this purpose, a Hidden Markov Model (HMM) is used (Rabiner, 1989). HMM is a model in which the state sequence – in our case, the rain or no rain period – is not directly visible, but variables, influenced by the states – here, the RSL attenuation – is visible. Each state has a probability distribution over the possible output taken. Therefore, the sequence of observations (RSL) generated by an HMM gives some information about the sequence of states (rain/no rain). In this case, the time series observations were modeled as a Markov process with two states: '0' (no-rain) and '1' (rain). In the HMM formulation, the state sequence is assumed to be a first order Markov process and the observations are assumed to be statistically independent given the states. To solve the problem of parameter estimation, in this case we use the well known Baum–Welch reestimation algorithm which involves iterative update and improvement of the model parameters based on the data (e.g.Baum and Petrie, 1966). However, since it is sensitive to the initial parameters, a decent initial estimate is necessary. Ideally we would use the rain indicator series from rain gauges in the region; however, since rain gauges are not always available we choose to initialize the parameters from the RSL data itself. As explained in Hadar (2009), in the case of opposite links (2 links along the same path), the correlation between attenuations at the two links tends to be high in times of rain because the rain causes well defined attenuation changes in a similar fashion for both links (usually the frequencies of the links are close) (Rahimi et al., 2003). Therefore, in the case of opposite links, the local correlation coefficient between the two links at each time step was computed, and was compared to a threshold to determine the

Table 1
Lists of all rain events, their dates, (+) the operational rain gauges, (−) the non-operational ones and (0) the dismantled rain gauges.

Rain events' period (local time)	Total hours (approx.)	Number of operating links	Rain gauge name						
			MTG Ramle [RG1]	Ramle West [RG2]	Modiin Center [RG3]	Modiin Shimshoni [RG4]	Maccabim [RG5]	Kfar Shmuel [RG6]	Talmie Yechiel [RG7]
22 December 2006 20:00 to 23 December 2006 20:00	24 h	42 links	+	+	+	+	+	−	**0**
26 December 2006 09:00 to 27 December 2006 21:00	36 h	40 links	+	+	+	+	−	+	**0**
31 December 2006 10:00 to 31 December 2006 18:00	8 h	50 links	+	+	+	+	−	+	**0**
05 January 2007 12:00 to 08 January 2007 02:00	62 h	44 links	+	+	+	+	−	+	**0**
29 January 2007 09:00 to 30 January 2007 23:00	38 h	47 links	+	+	+	−	+	−	**0**
03 February 2007 03:00 to 07 February 2007 10:00	103 h	40 links	+	+	+	−	+	−	**0**
09 February 2007 19:00 to 10 February 2007 10:00	15 h	50 links	+	+	−	−	−	−	**0**
26 February 2007 01:00 to 27 February 2007 04:00	27 h	35 links	+	+	+	+	−	−	**0**
26 March 2007 16:00 to 27 March 2007 10:00	18 h	49 links	+	+	+	+	+	−	**0**
31 March 2007 17:00 to 31 March 2007 22:00	5 h	60 links	+	+	+	+	+	−	**0**
3 May 2007 04:00 to 3 May 2007 14:00	10 h	34 links	+	+	−	+	−	−	**0**
12 May 2007 07:00 to 12 May 2007 18:00	11 h	63 links	+	+	+	+	−	−	**0**
19 December 2007 04:00 to 21 December 2007 04:00	48 h	69 links	+	+	+	+	**0**	+	**0**
3 January 2008 17:00 to 4 January 2008 20:00	27 h	69 links	+	+	+	+	**0**	+	**0**
22 January 2008 03:00 to 23 January 2008 15:00	36 h	64 links	+	+	+	−	**0**	+	+
26 January 2008 04:00 to 27 January 2008 04:00	24 h	67 links	+	+	+	−	**0**	+	+
28 January 2008 01:00 to 31 January 2008 13:00	84 h	65 links	+	+	+	−	**0**	+	+
11 February 2008 22:00 to 15 February 2008 04:00	78 h	63 links	−	+	+	−	**0**	+	+
18 February 2008 11:00 to 19 February 2008 09:00	22 h	64 links	−	+	+	−	**0**	+	+

initial wet and dry periods. The threshold, and the segment length (in minutes) on which the correlation coefficient was computed, were determined experimentally. A threshold of 0.6 was used and a segment length of 9 min. In the presence of rain, the attenuation tends to vary more rapidly (Goldshtein et al., 2009). Therefore, in the cases where an opposite link was not available, the standard deviation of the RSL was computed at each time step on a segment length of 9 min, and was compared to a threshold to determine the wet and dry periods. Since the links vary in their RSL values, a different threshold should be assigned to each link. Therefore, we took the threshold to be the mean of the RSL's standard deviation.

For a RSL time series of length T ($A_1 \ldots A_T$), the following procedure was carried out. First, by using HMM, the indicator sequence was generated as described above.

$$I_n = \begin{cases} 0, & \textit{no rain at time } n \\ 1, & \textit{rain at time } n \end{cases}.$$

At times of no rain, the dry-air RSL Z_n equals the RSL. i.e., $Z_n = A_n \forall n \in S_0$ where S_0 denotes the set of "dry times", or $S_0 = \{n : I_n = 0\}$. The values of Z_n at times of rain $\{Z_n : n \notin S_0\}$ were interpolated from $\{Z_n : n \in S_0\}$. Finally, the rain induced attenuation is given by $-(A_n - Z_n)$. The illustration of the dry\wet period identification is given in Fig. 2. Note that since this procedure allows accurate estimates of the wet–dry periods, no correction due to wet antenna attenuation (WAA) is included (as done by Zinevich et al., 2010). It is assumed that the errors caused by the WAA which can result in considerable overestimation of rain rate are captured from short no-rain periods between rainfall appearances and therefore inherently accounted for in the zero rainfall attenuation calculation.

However, for the rainy periods, proceeded by long dry periods (or for a first rainy period in an event), when the antenna is initially dry, the large errors may be encountered, decreasing toward the end of these rainy periods (can be seen in Fig. 2). In the Israeli climate, characterized by intensive convective rainstorms, frequently intermittent, the proportion of these rainy periods (e.g. preceded by more than 15 min of no-rain) may reach 30% over the entire amount of rainfall (this would be different for stratiform events). In this case, the rainfall will be overestimated, especially for short links that are affected by WAA to a larger extent. In practice, this effect does not expressed in any prominent overestimation (see Tables 2, 3), possibly because it is masked by other error sources (mismatch of actual power law coefficients vs. used ITU (2004) power law coefficients, spatial rainfall variation, etc., see Zinevich et al., 2010). The presented results did not involve any calibration. If WAA model is included and the WAA coefficients are calibrated (Leijnse et al., 2007a; Zinevich et al., 2010) on a sufficiently large dataset, this systematic deviation will be compensated. For direct estimation of WAA see for example Kharadly and Ross (2001), Leijnse et al. (2008), Minda and Nakamura (2005), Zinevich et al. (2010).

3.2. Single link vs. spatial reconstruction algorithm

As mentioned above, the first methodology simply takes the RSL data from the closest link, and after defining rain and no rain periods as described above, applies the power law to generate rainfall time series. Fig. 2 illustrates the steps necessary in this methodology. As opposed to this technique, where only information from a single link is used, in the spatial reconstruction algorithm, data from all nearby links surrounding a specific point (e.g. rain gauge location) is included. For this application, we followed the stochastic interpolation algorithm presented in Goldshtein et al. (2009). This algorithm, based on Shepard (1968) interpolation over an irregular grid, estimates the spatial distribution of rainfall at every time slot over a regular 2D data grid at the arbitrary spatial resolution, accounting for uncertainties of measurements of path-integrated rainfall due to

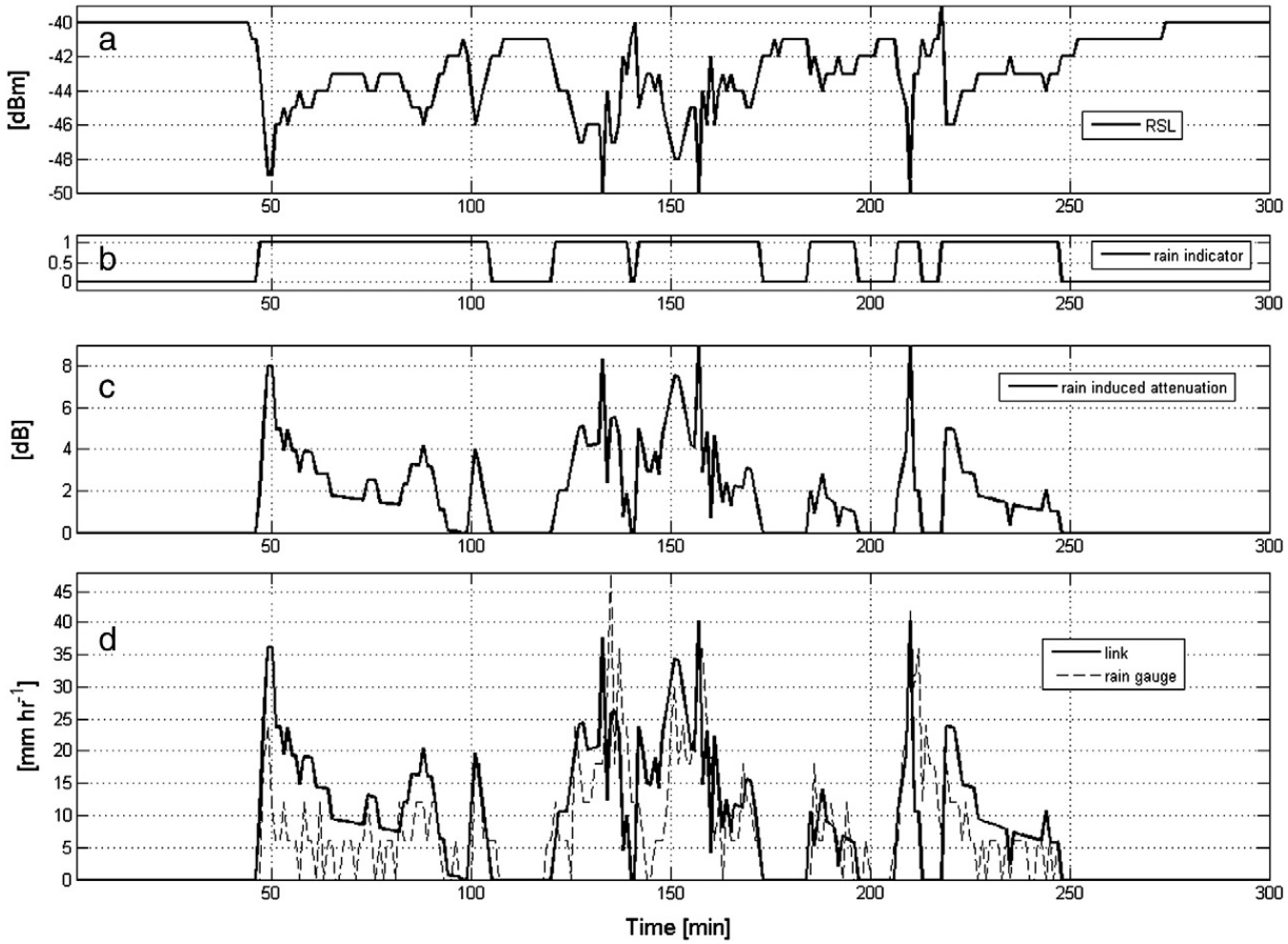

Fig. 2. A 3-hour example of the (a) RSL, (b) rain indicator, (c) rain induced attenuation and (d) rain estimated from the microwave link obtained by applying the power law (solid line) along with the rain gauge measurement (dashed line).

observation quantization. In fact, the effective spatial resolution of the technique is determined by the link density that varies in space considerably (see Fig. 1). Choosing the reconstruction pixel size to be 1×1 km^2 allows representing well the densest parts of the network.

Let $link_1, link_2, \ldots, link_N$ be the set of a given N terrestrial microwave links, where $link_i$ defined by the 5 parameters Lat_{i1}, Lon_{i1}, Lat_{i2}, Lon_{i2}, A_i is further explained. Each i_{th} $i=1,2,\ldots,N$ link is identified by latitude and longitude coordinates of its two edges – $(Lat_{i1}, Long_{i1}, Lat_{i2}, Long_{i2})$ and

Table 2
Average correlation, RMSE, Bias [mm h^{-1}] and Normalized RMSE between rain gauge measurements and nearest link measurements (upper line), and between rain gauge measurements and spatial estimated rain-rate in rain gauge location (lower line). Both calculations are performed at the 1 min and 10 min temporal resolutions. For all rain gauges, calculations are performed for each rainfall event separately and then combined.

Rain gauge name	One minute sample				Ten minutes samples			
	Normalized RMSE	Bias	RMSE	Corr	Normalized RMSE	Bias	RMSE	Corr
MTG Ramle (RG1)	3.90	−0.08	1.78	0.65	2.11	−0.11	1.02	0.84
	3.86	−0.06	1.70	0.77	1.83	−0.06	0.88	0.85
Maccabim (RG5)	4.26	−0.05	1.89	0.23	2.86	−0.05	1.20	0.61
	4.27	−0.01	1.89	0.23	2.44	−0.01	1.15	0.57
Modiin Center (RG3)	3.39	−0.25	2.22	0.50	1.80	−0.26	1.36	0.58
	3.39	−0.23	2.23	0.51	1.90	−0.19	1.49	0.76
Modiin Shimshoni (RG4)	2.70	−0.35	2.05	0.50	1.82	−0.35	1.36	0.77
	2.70	−0.37	2.09	0.64	1.74	−0.37	1.35	0.80
Ramle West (RG2)	4.26	−0.15	1.71	0.58	2.50	−0.15	0.98	0.82
	5.00	−0.06	1.80	0.64	3.10	−0.06	0.98	0.83
Kfar Shmuel (RG6)	2.67	−0.15	2.28	0.48	1.80	−0.15	1.55	0.69
	2.77	0.01	2.36	0.50	1.90	0.01	1.62	0.70
Talmie Yechiel (RG7)	4.00	0.22	2.36	0.35	2.45	0.19	1.51	0.67
	3.57	0.06	2.06	0.49	2.05	0.06	1.24	0.71

Table 3
Total rainfall accumulation [mm], averaged differences of rain accumulation in each rain gauge location for all rain events [mm] and averaged ratio of rain accumulation in each rain gauge location for all rain events. Number of rain events per gauge indicated in parenthesis. The total is calculated from all events together. The averages for all 7 rain-gauges are given at the bottom to provide an overall comparison.

Rain gauge name	Total rain accumulation			Average rain gauge vs microwave link		Average rain gauge vs interpolation point	
	Rain gauge	Microwave link	Interpolation point	Diff [mm]	Fractional bias	Diff [mm]	Fractional bias
MTG Switch Ramle (17)	349.8	494.6	356.8	8.5	0.41	0.4	0.02
Ramle West (19)	443.0	449.0	458.2	0.3	0.01	0.8	0.03
Modiin Center (17)	504.0	460.7	431.2	−2.7	−0.9	−4.6	−0.14
Modiin Shimshoni (11)	240.0	120.2	138.0	−12.0	−0.50	−10.2	−0.42
Maccabim (5)	124.7	109.2	110.8	−2.6	−0.12	−2.3	−0.11
Kfar Shmuel (10)	361.1	441.5	413.5	8.0	0.22	5.2	0.14
Talmie Yechiel (5)	164.9	248.1	206.1	16.6	0.50	8.2	0.25
Average	312.5	331.9	302.1	2.3	0.06	−0.3	−0.03

produces an observation vector $\underline{A}_i$, containing the time series of the recorded RSL values. The vector of path-integrated rainfall intensities $\underline{R}_i$ is calculated from $\underline{A}_i$ using the power law relation (Eq. (1)), according to the ITU parameterization[1] (1999).

Each microwave link is divided into M_i segments of equal length so that the rainfall intensity is assumed constant inside a segment. The midpoints of each segment represent data points with rainfall intensity at every time slot r_{ij}, $i=1,\ldots,N$, $j=1,\ldots,Mi$, and satisfy the constraints of the path-integrated measurement (here L_i is the length of the ith link):

$$R_i \cong \left(\frac{1}{M_i a_i}\sum_{j=1}^{M_i} a_i r_{ij}^{b_i}\right)^{\frac{1}{b_i}} \tag{2}$$

In order to reconstruct a two dimensional precipitation map the monitored area is marked by an $n\times n$ regular grid, so that each grid pixel is attributed with a region of influence Γ_i, (unit: km) and can be spatially analyzed. It should be noted that given the algorithm used in this study, variance decreases with link length.

Let θ denotes the rainfall rate in the middle of the pixel with coordinates(x,y) and let $[R_1,R_M]$ be a series of M spatial distributed rain rate data points, obtained from RSL measurements. The algorithm uses the modified Inverse Distance Weighted (IDW) interpolation over irregularly scattered points. It is important to notice that each link receives an additional weight, inversely proportional to the uncertainty of observation of path-integrated rainfall due to observation quantization:

$$\theta(x,y) = \frac{\sum_{i=1}^{N}\sum_{j=1}^{M}\left(W_{ij}+z\times\sigma_i^2\right)^{-1}\times r_{ij}}{\sum_{i=1}^{N}\sum_{j=1}^{M}\left(W_{ij}+z\times\sigma_i^2\right)^{-1}} \tag{3}$$

Here, σ_i^2 is the variance of uniform distribution of quantization error over the ΔdB quantization interval and z is a ratio constant, governing the contribution of quantization error. W_i is the inverse distance weighting function given by:

$$W_{ij}(x,y) = \begin{cases} \dfrac{\left(1-\dfrac{l_{ij}}{\Gamma}\right)^{\gamma}}{\left(\dfrac{l_{ij}}{\Gamma}\right)^{\gamma}}, & \dfrac{l_{ij}}{\Gamma}\le 1 \\ 0, & \dfrac{l_{ij}}{\Gamma}>1 \end{cases} \tag{4}$$

Where l_{ij} denotes the distance between the required estimated grid point θ at location (x,y) and sampled data point $d_{ij,\ i=1,\ldots,N,\ j=1,\ldots,Mi,}$ Γ is the radius of influence that depends on the spatial rainfall correlation properties. As part of a sensitivity analysis, we checked 1 km, 3 km and 6 km. The 1 km value provided the best results, however in reality did capture the spatial interpolation because most of the links are not within a 1 km radius from each other but rather are further away. The 6 km value created much noise and "false" rainfall. Based on these results, 3 km was chosen ($\Gamma=3$ km). The ratio constant z was set at 0.5 following Goldshtein et al. (2009).

The unknown variables r_{ij} are determined using an iterative Expectation–Maximization algorithm, where at each iteration k the expected θ is calculated given the current estimates of r_{ij} and then r_{ij} is re-estimated to minimize the mean square error (MSE) objective function, subject to the constraint Eq. (2) for every link $i=1,\ldots,M_i$:

$$\left\{r_{i1},\ldots,r_{iM_i}\right\}^k = \underset{\mathrm{r:(2)}holds}{\arg\max}\left[-\sum_{i=1}^{N}\int\left(r_i^{k-1}(x)-\theta(x)\right)^2 dx\right] \tag{5}$$

where $\{r_{i1},\ldots,r_{iM_i}\}^k$ is the newly estimated distribution of rainfall intensities (grid points spaced based upon the chosen region of influence) along the i_{th} link and x denotes a location along the link where $r_i^{k-1}(\mathrm{x})$ is a piecewise-linear estimate of point rainfall (at location x) along the link. N, as mentioned above, is a set of terrestrial microwave links. The constrained optimization is done using a standard technique of Lagrange multipliers. We start by assuming that the rain rate is uniformly distributed along each link integrated path and derive the spatial data point's rain rate vector from their parent link rain rate vector. More details are given in Goldshtein et al. (2009).

[1] Specific attenuation model for rain for use in prediction methods, The Radio Communications Agency of the International Telecommunications Union, ITU-R Recommendation P.838-1, 1999.

The major advantage of this algorithm is that it can easily be adapted to various microwave network configurations, with the calibration of constants z, and Γ. Its major limitation arises from the fact that the Expectation–Maximization algorithm finds only local maxima. With regard to the practical applicability of the method, the computation time of the inverse distance interpolation method (Eq. (3)) is proportional to the area, while the computation time of the rain/no-rain identification algorithm and the iterative algorithm (Eq. (5)) is proportional to the total length of the links. For modern CPUs, the algorithm can easily be implemented in the real-time. For large areas, the algorithm can also be easily parallelized for processing of different areas on different CPUs.

4. Results

The rainfall time series obtained from microwave links are compared with rain gauges at seven different locations (Fig. 1) based on two different microwave-derived rainfall estimates: path-averaged rainfall, measured by a nearby link, and the result of spatial interpolation using the modified Inverse Distance Weighting (IDW). The skills of the methods were calculated separately for each rain event in all of the rain gauge locations, for time intervals of both 1-min and 10-min average samplings of microwave links. The actual RSL values measured by the cellular companies are 1-minute average samplings. The 10-minute average values are calculated based on the 1-minute values. For each set of values the appropriate power law parameters, a and b (see Eq. (1) above) were chosen.

For each of the rain gauges a number of skill parameters were calculated including: (1) temporal correlation coefficient, providing insight into the potential of rainfall estimates using the proposed technique, (2) bias and RMSE, giving the performance estimates in absolute units and (3) total rain accumulation statistics. Summary of the correlations, biases, and RMSE results for the rainfall intensity (mm/h) based on the 2 methodologies are presented in Table 2.

Fig. 3 shows an example of the comparison between a rain gauge and the two methodologies for a rain event occurring on Dec. 26, 2006. Analysis of these results follows in the next sections.

4.1. Analysis of correlations results

The Ramle West [RG2] and MTG Ramle [RG1] rain gauges, located inside the city of Ramle show, as expected, the highest correlation with microwave-derived rainfall estimates reaching 83% and 85% over all rain events respectively for the 10 min time period. The gauge RG1 is located in the center of the city surrounded by a star-like construction of microwave links (Fig. 1) while the RG2 gauge is located 1.4 km west of RG1 and 1.2 km north east of the Ramat Dan microwave link. Also, not unexpected, the lowest correlations between rain gauge point measurements and microwave rainfall estimates are at the Maccabim [RG5] rain gauge, located on the eastern border of the research area with a very small link-density. In the case of spatial interpolation, the estimates of microwave rainfall at the RG5 location are produced by only one microwave link, located 1.7 km west to the RG5 rain gauge and over 4 km from the next closes link in Modiin Titora (TT). If the TT link was not operational during a rain event, it was not included in the RG5 radius of influence (Γ). In the Modiin area, there are two rain gauges (RG3 and RG4) and up to 4 operating microwave links. The best average correlation of 0.80 was achieved at RG4, located in the middle of a long microwave link. The gauge RG6 is located in the rural area, 7 km east of Ramle and 4 km from the city of Modiin; as a result, the best average correlation in RG6 is only 0.7. The gauge RG7 is a rural station. It is located 2.4 km north-west from the southern group of microwave links around Kiryat Malachi switch. The nearest link is located 1.3 km east to the rain gauge; with the average correlation is 0.71.

4.2. Analysis of root mean square error and bias results

Table 2 shows that rain gauge RG1, with the highest link density, has the lowest average RMSE (0.88 mm h^{-1}) along with a relatively small bias (−0.06 mm h^{-1}). In the Modiin area, the lowest average RMSE (1.35 mm h^{-1}) is found for RG4, with bias of−0.37 mm h^{-1}. The lower skill of the results for RG4 as compared to RG1 (Ramle) is due to the lower number of microwave links available (maximum of 4 working links). For many cases, only one microwave link (Mavo Modiin link) was available for the comparison of the 3 rain gauges in that area (RG3, RG4, RG5). The negative bias that can be seen in the 6 northern rain gauges locations indicates that there is underestimation of the microwave rainfall compared to the nearest rain gauge. This is potentially due to the strict estimation of zero rainfall attenuation algorithms as described in Section 3.1. The bias is systematically lower in the spatial interpolation methodology. One station (RG7) exhibits a positive bias when compared both to the nearest microwave link and using the spatial interpolation result. This is due to the location of the rain gauge – it is located on a farm a few meters from a row of trees, north-west of the southern group of microwave links. Hence, there could have been some blocking of the gauge rainfall located on the ground which resulted in underestimation at the gauge as compared with the microwave rainfall estimates located above the ground. Rain gauges RG1, RG2, RG3, RG4 and RG6 are located in open areas with no environmental disturbances. In addition to RG7, the only other rain gauge with potential environmental interference in RG5 (Maccabim) located on a private home in the area. . It is surrounded by trees and there are some disturbances from the west, though it is important to note that it is higher than the surrounding trees.

4.3. Analysis of rain accumulation results

For hydrological implication such as surface run off, urban flooding and flash floods, the amount of total accumulated rain over a specific time period is of great value. While the correlations and error statistics were based on 1-min and 10-min average samplings of microwave link with the rain gauge time series, here we compare the total rainfall accumulated produced by the three methods (as measured by rain gauges and both estimates from the attenuation measurements of the microwave networks). This was performed for all 7 rain stations and for all recorded rainfall events (see Tables 1 and 3). Two ways for assessing the ability of the microwave facilities to estimate the total rain accumulation amounts will be employed. First, the difference between the integral amounts

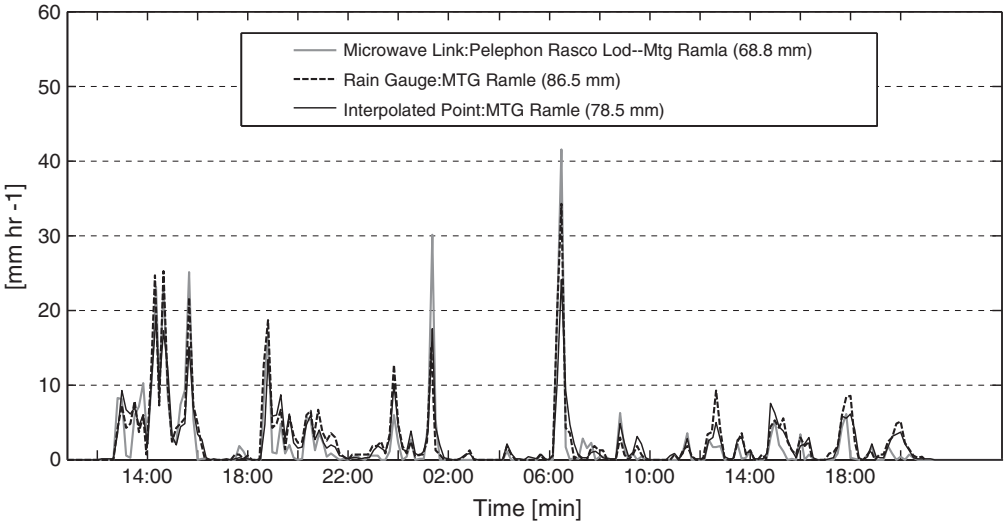

Fig. 3. A comparison of rainfall measurements from a rain gauge, single link, and interpolated link for rainfall on Dec 26, 2006. Total rain from this event is shown for each measuring method. The rain gauge RG1 (see Fig. 1) is very close to the chosen single link and is located in an area surrounded by multiple links (see Fig. 1). Hence, correlations between the rain gauge measurements and both methodologies are very high in this case (0.91 for single link and .094 for interpolated link).

of the rainfall (in mm) produced by the microwave links and all rain gauges for each rain event are calculated, yielding the absolute error. To estimate the relative differences between microwave rainfall and rain gauges, also the fractional bias of the total accumulated amounts are calculated (Table 3) The total amounts (in mm) shown in Table 3 complement those shown in Table 2 which depicts on rainfall intensity (in mm/h) averaged over the many rainfall events. It should be noted that for the average rainfall intensity calculations in Table 2 the statistics shown (RMSE, normalized RMSE, bias, and correlation) are computed for each event separately and then averaged afterward (Table 2) as opposed to the total amounts (Table 3) where fractional bias is calculated from all events combined.

The results show that averaging for the 7 rain stations provides the total difference between the microwave links and the rain gauges of only 2.3 mm, and the total difference between the interpolated rainfall and the rain gauges is underestimated by only 0.3 mm. The total averaged ratio between the microwave links and the rain gauges is overestimated by only 6%, and the total averaged ratio between the interpolated points and the rain gauge is underestimated by only 3%. For both methodologies, the best average ratio and the smallest average difference were achieved for RG2 where the link density is the highest (Table 3). RG1 shows the best average ratio and average difference when comparing the interpolated rainfall to the rain gauge. In stations RG3, RG4 and RG5 (Fig. 2, the Modiin area), there is an underestimation in all 3 rain stations. The lowest average ratio of 0.5 for the nearest link and 0.57 for the interpolated point is at RG4. In contrast, the gauges RG6 and RG7 in the rural area are characterized by larger errors, i.e., an overestimation with RG7 reaching the average ratio values of 1.51 and 1.25 compared with the closest microwave link and to the interpolated point, respectively. As can be seen there are large biases in the results. This can be explained due to the location of the rain gauges, the distance from the various links and the surrounding environmental disturbance for measuring rainfall.

5. Discussion and conclusions

Microwave rainfall measurements of near-surface rainfall may have numerous applications — from urban hydrology, flood warning and development of efficient cloud seeding techniques to improving efficiency in telecommunications. Important meteorological benefits of the technique are accurate mapping of near-surface precipitation over wide areas, including currently unmapped areas with reliable rainfall measurements such as steep topography and dense urban region. Measuring high spatial resolution of near-surface rainfall at the temporal resolution of 1 min is another unique advantage of the commercial microwave network, demonstrated in this study. A larger time interval of even 5 min, typical for radars, can be some source of errors (Morin et al., 2003; Piccolo and Chirico, 2005). This study explores the concept of obtaining rainfall measurement from commercial microwave communication links using two techniques and applied to two full winter seasons in Israel (19 individual rain events). In general, the results indicate that the skill of both methods improve as the density of the links increases. The two stations showing the highest skill are RG2 (Ramle West) and RG3 (Modiin Center), both surrounded by multiple links with various lengths. However, it should be noted that these are also the two stations where the single link methodology proved superior to that of multiple link interpolation. This could be due to the fact that the interpolation methodology included information from longer links potentially causing some shift in the rain timing and intensity. For the three links in the Modiin area (RG3, RG4, and RG5) the results from RG4 are substantially weaker, in spite of the relative proximity of the stations to the links. This can be attributed to the orientation of the link(s) being used. In general, convective storm producing fronts blow in from the south-west. A link oriented parallel to the front measures rainfall in a substantially different manner i.e., high rain intensity over a short period, while with a perpendicular orientation of the link one would expect lower rainfall intensity over a longer period. The impact of the link

orientation to rainfall measurements is the topic of a separate study. These results indicate that the specific location of rain gauges and characteristics of the surrounding links can play a significant role depending on type of rainfall. Additionally, since both methods suggest microwave link density to be the limiting skill factor, for rural areas, where the cellular network is sparse, improved methodologies are warranted. Further discussion of these issues can be found in Zinevich et al. (2009) and Zinevich et al. (2010).

Acknowledgments

This work was supported by a grant from the Yeshaya Horowitz Association, Jerusalem. The authors would like to thank our colleagues: O. Goldshtein, N. David and H. Messer for their useful advice and discussion. We are deeply thankful to A. Shilo, E. Moshayov and N. Deval (Pelephone) for their cooperation and help in providing us with the microwave data at no charge and helping with the installations of the rain gauges. Additional support was provided by the GLOWA-Jordan River BMBF and MOS support as well as the EU-CIRCE projects. We also like to thank D. Dreamler and his crew at Israel Electrical Company, for their cooperation and their vital help in the installation of rain gauges. Comments from two anonymous reviewers have greatly improved the manuscript.

References

Atlas, D., Ulbrich, C., 1974. The physical basis for attenuation–rainfall relationships and the measurements of rainfall parameters by combined attenuation and radar methods. J. Rech. Atmos. 8, 275–298.

Atlas, D., Ulbrich, C., 1977. Path- and area-integrated rainfall measurement by microwave attenuation in the 1–3 cm band. J. Appl. Meteor. 16, 1322–1331.

Baum, L.E., Petrie, T., 1966. Statistical inference for probabilistic functions of finite state Markov chains. Ann. Math. Stat. 37, 1554–1563.

Berne, A., Uijlenhoet, R., 2007. Path-averaged rainfall estimation using microwave links: uncertainty due to spatial rainfall variability. Geophys. Res. Lett. 34 (7), L07403.

David, N., Alpert, P., Messer, H., 2009. Technical Note: novel method for water vapour monitoring using wireless communication networks measurements. Atmos. Chem. Phys. 9 (7), 2413–2418.

Giuli, D., Facheris, L., Tanelli, S., 1999. Microwave tomographic inversion technique based on stochastic approach for rainfall fields monitoring. IEEE Trans. Geosci. Remote. Sens. 37 (5), 2536–2554.

Goldreich, Y., 2003. The Climate of Israel: Observation. Springer Research and Application. 298 pp.

Goldshtein, O., Messer, H., Zinevich, A., 2009. Rain rate estimation using measurements from commercial telecommunications links. IEEE Trans. Signal Process. 57 (4), 1616–1625.

Grum, M., Kraemer, S., Verworn, H., Redder, A., 2005. Combined use of point rain gauges, radar, microwave link and level measurements in urban hydrological modeling. Atmos. Res. 77 (1–4), 313–321.

Hadar, U., 2009. 'High-order hidden markov models with applications to rainfall estimation from cellular network measurements'. M.Sc. Thesis Thesis, University of Tel Aviv, School of Electrical Engineering, Tel Aviv.

Holt, A., Goddard, J., Upton, G.I., Willis, M., Rahimi, A., Baxter, P., Collier, C., 2000. Measurement of rainfall by dual-wavelength microwave attenuation 36 (25), 2099–2101 Electron. Lett. 36 (36), 25.

Holt, A., Kuznetsov, G., Rahimi, A., 2003. Comparison of the use of dual-frequency and single-frequency attenuation for the measurement of path-averaged rainfall along a microwave links. IEEE Proc.-Micro. Antennas Propag. 150 (5), 315–320.

International Telecommunication Union Recommendation, 2004. ITU-R P.838–2 Specific attenuation model for rain for use in prediction model.

Jameson, A., 1991. A comparison of microwave techniques for measuring rainfall. J. Appl. Meteor. 30, 32–54.

Kharadly, M.M.Z., Ross, R., 2001. Effect of wet antenna attenuation on propagation data statistics. IEEE Trans. Antennas Propag. 49 (8), 1183–1191.

Krämer, S., Verworn, H., Redder, A., 2003. Microwave links — a precipitation measurement method filling the gap between rain gauge and radar data? 6th Intl. Workshop on Precipitation in Urban Areas.

Krämer, S., Verworn, H., Redder, A., 2005. Improvement of X-band radar rainfall estimates using a microwave link. Atmos. Res. 77, 278–299.

Leijnse, H., Uijlenhoet, R., Stricker, J., 2007a. Hydrometeorological application of a microwave link: 2. Precipitation. Water Resour. Res. 43, W04417.

Leijnse, H., Uijlenhoet, R., Stricker, J., 2007b. Rainfall measurement using radio links from cellular communication networks. Water Resour. Res. 43 (3), W03201.

Leijnse, H., Uijlenhoet, R., Stricker, J., 2008. Microwave link rainfall estimation: effects of link length and frequency, temporal sampling, power resolution, and wet antenna attenuation. Adv. Water Resour. 31, 1481–1493.

Messer, H., 2007. Rainfall monitoring using cellular networks. IEEE Signal Process. Mag. 24 (3), 144+.

Messer, H., Zinevich, A., Alpert, P., 2006. Environmental monitoring by wireless communication networks. Science 312 (5774), 713–716.

Minda, H., Nakamura, K., 2005. High temporal resolution path-average rain gauge with 50-GHz band microwave. J. Atmos. Oceanic Technol. 22, 165–179.

Morin, E., Krajewski, W.F., Goodrich, D.C., Gao, X., Sorooshian, S., 2003. Estimating rainfall intensities from weather radar data: the scale dependency problem. J. Hydrometeorol. 4, 782–797.

Piccolo, F., Chirico, G.B., 2005. Sampling errors in rainfall measurements by weather radar. Adv. Geosci. 2, 151–155.

Rabiner, L.R., 1989. A tutorial on hidden Markov models and selected applications in speech recognition. Proc. IEEE 77 (2), 257–286.

Rahimi, A., Holt, A., Upton, G., Cummings, R., 2003. The use of dual-frequency microwave links for measuring path-averaged rainfall. J. Geophys. Res. 108 (D14).

Rahimi, A., Holt, A., Upton, G., 2006. Attenuation calibration of an X-band weather radar using a microwave link. J. Atmos. Oceanic Technol. 23 (3), 295–405.

Rincon, R., Lang, R., 2002. Microwave link dual-wavelength measurements of path-average attenuation for the estimation of drop size distributions and rainfall. IEEE Trans. Geosci. Remote. Sens. 40 (4), 760–770.

Shay-Al, Y., Alpert, P., 1991. A diagnostic study of winter diabatic heating in the Mediterranean in relation to cyclones. Quart. J. Roy. Meteor. Soc. 117, 715–747.

Shepard, D., 1968. A two-dimensional interpolation function for irregularly-spaced data. ACM National Conf. 517–524. doi:10.1145/800186.810616.

Upton, G., Hold, A., Cummings, R., Rahimi, A., Goddard, J., 2005. Microwave links: the future of urban rainfall measurement? Atmos. Res. 77 (1–4), 300–312.

Upton, G., Cummings, R., Holt, A., 2007. Identification of melting snow using data from dual-frequency microwave links 1(2), 282–288. Microw. Antennas Propag. 1 (2), 282–288.

Zinevich, A., Alpert, P., Messer, H., 2008. Estimation of rainfall fields using commercial microwave communication networks of variable density. Adv. Water Resour. 31 (11), 1470–1480.

Zinevich, A., Messer, H., Alpert, P., 2009. Frontal rainfall observation by a commercial microwave communication network. J. Appl. Meteorol. Climatol. 48 (7), 1317–1334.

Zinevich, A., Messer, H., Alpert, P., 2010. Prediction of rainfall intensity measurement errors using commercial microwave communication links. Atmos. Meas. Tech. 3, 1385–1402.